Journal of
Marine Science and Engineering

MDPI

Article

Nearshore Waves and Littoral Drift Along a Micro-Tidal Wave-Dominated Coast Having Comparable Wind-Sea and Swell Energy

Jesbin George, V. Sanil Kumar *, R. Gowthaman and Jai Singh

Ocean Engineering Division, CSIR-National Institute of Oceanography (Council of Scientific & Industrial Research), Dona Paula-403 004 Goa, India; jgeorge@nio.org (J.G.); rgowtham@nio.org (R.G.); jsingh@nio.org (J.S.)
* Correspondence: sanil@nio.org

Received: 1 December 2019; Accepted: 12 January 2020; Published: 18 January 2020

Abstract: The nearshore wave characteristics and variations in littoral drift (longshore sediment transport; LST) are estimated based on different approaches for four years along the Vengurla coast, with comparable wind-sea and swell energy assessed. The waverider buoy-measured data at 15 m water depth is utilized as the input wave parameters along with the reanalysis model data, and the numerical wave model Delft-3D is used for estimating the nearshore wave parameters. The relative contribution of wind-seas and swells on LST rates are specifically examined. The clear prevalence of west-southwest waves implies the prevalence of south to north longshore sediment transport with net transport varying from 0.19–0.37 $\times 10^5$ m^3/yr. LST is strongly dependent on the breaker angle and a small change in the wave direction substantially alters the LST, and hence reanalysis/model data with coarse resolutions produce large errors (~38%) in the LST estimate. The annual gross LST rate based on integral wave parameters is only 58% considering the wind-seas and swells separately, since the wind-sea energy is comparable to swell energy, and the direction of these two systems differs significantly.

Keywords: coastal processes; longshore sediment transport; nearshore modelling; swells; wave characteristics; wind-seas

1. Introduction

Coastal zones are the most dynamic regions due to the release of energy by the surface gravity waves (hereafter waves). The waves propagating into the shallow water transform due to reflection, refraction, bottom friction, shoaling and breaking. When refracted, oblique waves reach the shore; the alongshore wave energy flux induces a net sediment transport whose gradients are responsible for shoreline evolution [1]. Breaking waves in the surf zone make an additional sediment stirring effect, caused by the breaking-induced flows, enhanced turbulent kinetic energy in the water column, and pore pressure responses in the sediments [2]. Knowledge of the physical processes in the nearshore region that impact sediment transport is essential to understand the erosion/accretion processes that mainly regulate the coastline stability [3]. Substantial morphological changes occur in sandy beaches due to the action of waves, currents, and tides, often controlled by the height and length of the nearshore waves. This morpho-dynamic change can be observed on different timescales and may vary daily, monthly and even yearly. The temporal variations in the littoral system are observed due to variations in the wave climate, and the change in the direction of longshore sediment transport (LST) is mainly due to change in the wave direction [4–6]. The wave direction can vary due to the changes in the offshore wave climate or because of the variations in the nearshore bathymetry [7–9]. Quantitative processes and coastal evolution through numerical modelling are now possible due to the significant

advances in understanding the physical processes and mathematical modelling techniques over the last few years [8]. One-dimensional morphology evolution models consider sediment transport along the longshore dimension based on several simplifying assumptions. The joint application of a calibrated wave propagation model, the LST equation and the one-line model constitutes a management tool for predicting the evolution of these complex coastal settings [5]. Bergillos et al. [6] used an integrated methodology to predict the plan view response of a deltaic coast (Guadalfeo, southern Spain) over a two-year period forced by different nourishment scenarios of coastline morphology, input LST and nourished sediment size.

During the past few decades, several methods have been developed for the computation of LST, and most of them are the bulk transport formulas—explicit equations based on simplified representations of physical processes that depend on the empirical coefficients. Bulk transport methods provide an estimate of the integrated LST rate (LSTR) over the whole profile with few input parameters. Many studies [10–12] indicate that transport is proportional to the energy flux of the longshore component of wave power for fully developed transport conditions. Komar and Inman [13] used the field-measured waves and found that the immersed weight of LSTR is directly proportional to the longshore component of wave energy flux. Smith et al. [14] reported that the LST estimation using the Coastal Engineering Research Centre (CERC) [15] has an accuracy of about 30–50%, and that the coefficient K of 0.39 is also found to overestimate the LSTR by 7 to 8 times for spilling breakers and by more than a factor of three for plunging breakers. Chempalayil et al. [16] studied various empirical equations and they found that the CERC equation shows a similarity in two locations having different nearshore characteristics, whereas the equation proposed by Walton Jr and Bruno [17] and Kamphuis [18] resulted in a vast difference in the values of LSTR due to the change in the nearshore parameters. Samaras and Koutitas [19] performed a review on studies regarding the comparative analysis and evaluation of the efficiency of 18 LST rate formulae and reported that the Kamphuis (1991) formula performed well against laboratory measurements. They also intercompared the CERC formula, the Bayram et al. [20] formula and the Kamphuis [18] formula as part of a properly adapted 1-D shoreline evolution model.

Shanas and Kumar [4] and Kumar et al. [21] studied four bulk formula (CERC, Kamphuis, Walton & Bruno and Komar) for the estimation of LSTR with the nearshore wave parameters based on wave transformation model Delft-3D as input and they observed that the estimation based on Kamphuis is close to the measured values. Prediction effect of the CERC formula gradually decreases from the open coast to the sheltered zone, whereas the Kamphuis approximation is reasonable for all types of coastal zones. The LSTR at different locations along the west coast of India based on measured wave data has been investigated by various researchers and iz reported to be between 1.4×10^5 and 7.0×10^5 m^3/yr (Table 1). The LSTR estimate based on the Kamphuis [18] formula, which includes all the responsible parameters like the wave period, beach slope, and sediment grain size, is found to be a reliable estimate for the west coast of India [4,16]. Hence, the same is used in the present study.

Studies conducted in the eastern Arabian Sea indicate that due to the co-existence of swells and wind-seas, the wave spectrum is bimodal for most of the time [22–24]. The predominance of wind-seas and swells were also reported in the eastern Arabian Sea [25]. In most of the studies, the integral wave parameters resulting from the combined wind-seas and swells are used in the estimation of the LSTR along with the wave direction corresponding to the spectral peak [4,16,21]. However, in areas like the eastern Arabian Sea, where the wind-seas and swells have different directions [24], the estimation based on LSTR considering the wind-seas and swells separately needs examination. Also, it is essential to understand changes in the nearshore wave climate and LST in an annual cycle as the nearshore regions up to 10 km from the coast in the eastern Arabian Sea are intense fishing zones and this area is also extensively used for tourism-related activities and development of marine facilities. The relative contribution of wind-seas and swells on LSTR are not specifically examined in all previous studies and the LSTR estimate is based on the integral wave parameters. To the best of our knowledge, no previous studies were done along this region to estimate LST and wave climate using continuously measured

data for more than a year. Thus, the present study aims to understand the changes in the nearshore wave parameters and the LSTR and investigates the influence of wind-seas and swells on the LST.

Table 1. Longshore sediment transport rate (LSTR) along the west coast of India.

Location	Net Sediment Transport Rate (10^6 m^3/yr)	Gross Sediment Transport Rate (10^6 m^3/yr)	Data Used, Period and Method Used	Formula Used	Reference
Maharashtra Ganpatipule	0.08 0.01 0.05	0.23 0.04 0.19	Measured wave data (2011–2016), Delft 3D model	CERC Kamphuis Walton & Bruno	[26]
Maharashtra Vengurla	0.008	0.11	Measured wave data Jan–Dec (2015), LITDRIFT Model	-	[27]
Karnataka Karwar	0.04	0.14	Measured wave data, SWAN wave model Feb 2009–Jan 2010	Kamphuis	[28]
Karnataka Pavinkurve Kasargod	0.46 0.29 0.20 0.47 0.30 0.18	0.7 0.4 0.4 0.7 0.5 0.2	Measured wave data, REFDIF-I wave model & empirical equation Jan–Dec 2009	CERC Walton&Bruno Komar CERC Walton&Bruno Komar	[16]
Karnataka Kundapura	0.137 0.178 0.163 0.125	0.334 0.349 0.310 0.343	Measured wave data, Delft-3D wave model & empirical equation Jan–Dec 2011	CERC Kamphuis Walton&Bruno Komar	[4]
Karnataka Malpe	1.12 0.82 0.33 0.89	1.26 0.92 0.35 1.01	Measured wave data, Delft-3D wave model & empirical equation Jan–Dec 2009 and 2011)	CERC Walton&Bruno Kamphuis Komar	[21]

2. Study Area

The west coast of India is subjected to high wave activity during the Indian summer, i.e., southwest monsoon (June–September, hereafter monsoon) and during this period most of the sandy beaches undergo erosion [29]. Typically, the beach restores its equilibrium state during the post-monsoon period [28]. The study area is off Vengurla, situated along the central west coast of India (location 15.87° N to 73.63° E) (Figure 1). The east side of this coastal segment is bound by the Western Ghats mountain range, while the Arabian Sea extends along its west side. It is surrounded by a semicircular range of hills and is exposed to open ocean waves from northwest to south. The nearest landmass is ~1500 km in the northwest, ~2000 km in the west, ~4000 km southwest and ~9000 km in the south [30]. The Vengurla coast is characterized by a tropical climate, and the annual precipitation is ~3100 mm [31]. Nature and spatial distribution of geomorphic features along the coast indicate that the study area is a scene of neotectonic activity [32]. The tidal regime of this region is 2.3 m during spring tide and 1.3 m during neap tide. A longshore current velocity of 0.5 m/s was reported [31]. High wave activity (seasonal average H_s ~2 m) is experienced during monsoon and calm wave conditions (H_s < 1 m) during the remaining period of the year [25]. Based on Davies classification [33,34], the wave and tide data together exhibit that the study area is on a microtidal wave-dominated coast and the predominant breaker is a plunging breaker with multiple breakers [35].

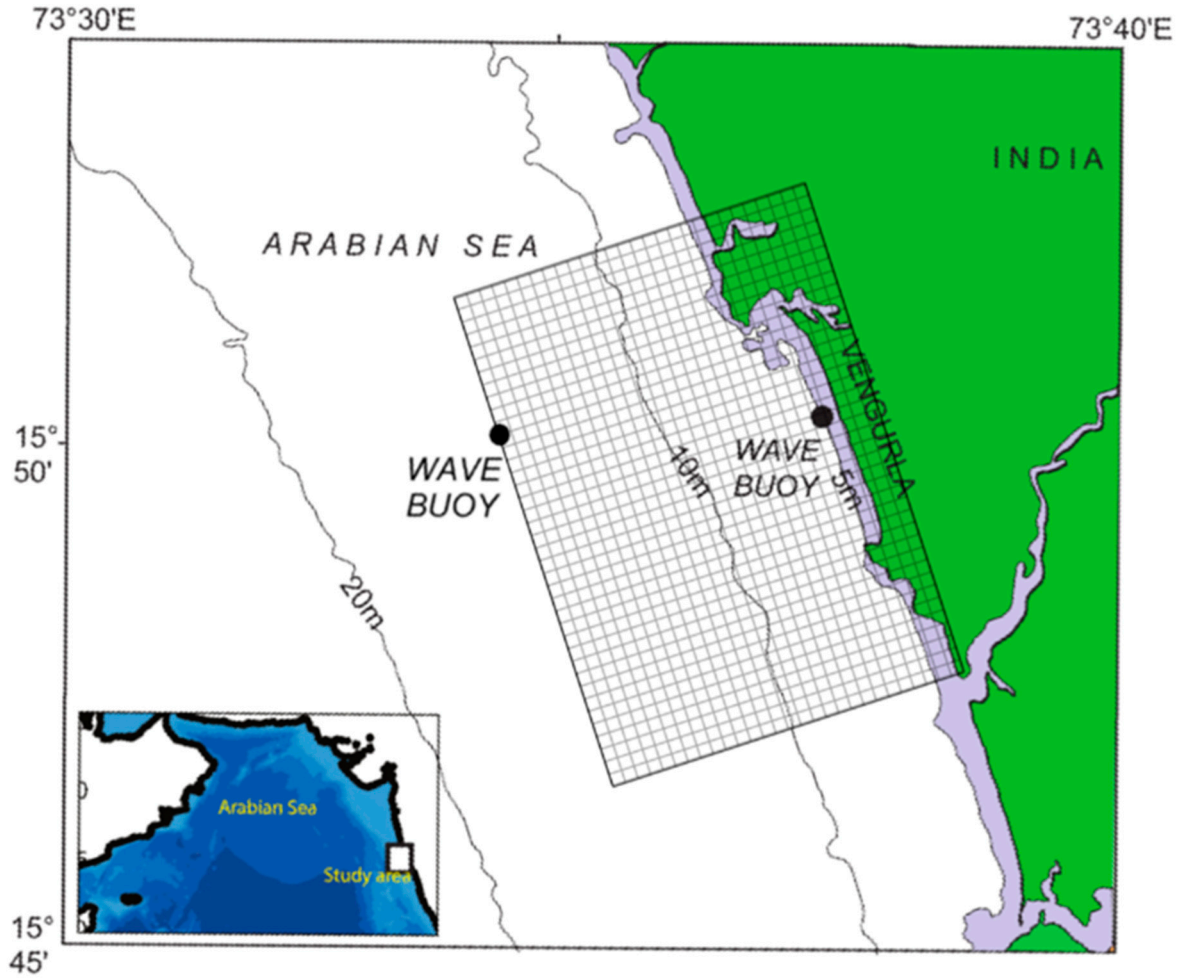

Figure 1. Study area in the eastern Arabian Sea showing the locations of the wave rider buoys at 15 and 5 m water depth. The rectangular box represents the model grid and its boundaries.

3. Data and Methods

The bathymetry of the study area was obtained by merging the nearshore measured bathymetry data from coast to 5 m water depth with the digitized naval hydrographic chart No. 2043 [36]. During September 2014 to August 2015, the median size of the nearshore sediment (D_{50}) was obtained in a monthly interval. The D_{50} was extracted by the following geometric (modified) Folk and Ward [37] graphical measures using GRADISTAT: a grain analysis package [38] and the size distribution of sediments was obtained using an electromagnetic sieve shaker. Wave data was collected at 30 min intervals at 15 m from September 2014 to August 2018 and is used as an input for the model. The WAVE module of the Delft3D model [39] was used as the numerical model for nearshore wave transformation to estimate the breaker wave parameters. This numerical model is based on the SWAN model [40], a third-generation phase-averaged wave model based on a fully spectral representation of the action balance equation and it can accurately reproduce the main wave propagation processes in coastal areas, e.g., shoaling, refraction due to bottom and current variations, transmission/blockage through/by obstacles, white capping, bottom friction, depth-induced wave breaking, non-linear wave–wave interactions, and wind effects [41]. This model was previously employed along several locations in the central west coast of India [4,19,26,42] and researchers have described in detail the wave transformation model, grid generation, attributes, input parameters etc., which are the same for the present study. Significant wave height (H_s), mean wave direction and mean wave period (T_{m02}) are the input wave parameters used in the model. Other input variables used in the model are JONSWAP bottom friction coefficient (0.067 m^2 s^{-3} [43]), depth-induced breaking (Alpha (1) and Gamma (0.73), [44]),

and nonlinear triad interactions (Alpha and Beta being 0.1 and 2.2, respectively) based on Lumped Triad Approximation model [45]. The model simulations were carried out in stationary mode and have three boundaries: (1) open boundary to the west, (2) closed boundary to the east, and (3) lateral boundaries to the north and south. The model has 24 frequencies between 0.05–1 Hz and the directional resolution of the model is 10 degrees. No wind fields were included in the model since the domain is small. Furthermore, sea level changes due to the influence of tide were also not considered. The domain was divided into 200 × 450 grid points with a grid spacing of 20 m each along x and y directions. The method suggested by Portilla et al. [46] was used to separate wind-seas and swells from the measured data. The 1-D separation algorithm was based on the assumption that the energy at the peak frequency of a swell cannot be higher than the value of a Pierson–Moskowitz (PM) spectrum with the same frequency. If the ratio between the peak energy of a wave system and the energy of a PM spectrum at the same frequency is above a threshold value of 1, the system is considered to represent wind-sea, else it is taken as swell. A separation frequency fc is estimated following Portilla et al. [46] and the swell and wind-sea parameters are obtained for frequencies ranging from 0.025 Hz to fc and from fc to 0.58 Hz, respectively. The 4 years of simulations carried out in a workstation (HP Z 800) took a period of 2 months and the output was stored to a 500 GB hard disk. ERA-Interim data [47] from September 2014 to August 2015 of significant wave height (H_s), mean wave period and mean wave direction at six-hour intervals were also obtained with a spatial resolution of 0.5° × 0.5° to compare the LSTR estimated with the measured and reanalysis data. For wave transformation based on ERA-I data, the domain was first divided into 400 × 250 points with a grid spacing of 100 m and 75 m respectively. This low-resolution grid was nested to a high-resolution grid (450 × 450) with a grid spacing of 10 m each along x and y direction. The model simulation was carried out for four years from 1 September 2014 to 31 August 2018, and the transformed breaking characteristics were extracted by considering the breaking criteria (H_b/h_b = 0.78; [15]). These extracted output parameters, breaking wave height (H_b), T_{m02} and wave breaking angle were used for the calculation of LSTR.

The LST is estimated based on the bulk transport formula developed by Kamphuis [18]. The Kamphuis equation includes the wave period, which influences wave breaking and grain size, which affects the sediment motion. Due to the orientation of the coastline at 22° with respect to the west, a wave direction less than 248° generates northerly LST and is taken as positive and wave direction more than 248° generates southerly LST and is taken as negative.

$$Q_{LST} = 7.3{H_b}^2{T_p}^{1.5}{m_b}^{0.75}{d_{50}}^{-0.25}\sin^{0.6}(2\theta) \quad (1)$$

In Equation (1), Q_{LST} = the longshore sediment transport in volume per unit time, H_b = breaking wave height (m), T_p = peak wave period (s), m_b = slope of the bottom in the surf zone, d_{50} = sediment median grain size (mm), and θ = the angle between the incident wave ray and local shoreline (deg).

4. Results and Discussion

4.1. Wave Characteristics at 15 m Water Depth

As expected, high waves are observed during the monsoon, since the Arabian Sea is the key region of strong air–sea interactions associated with the monsoon. The highest H_s observed (~5 m) is in June 2015 and July 2018, and during the monsoon, H_s ranged from 0.5 to 5 m with an average value of 1.8 m (Figure 2a). They were predominantly from the west–southwest direction (Figure 3) due to the dominance of swells in the west coast of India during this season [21,48]. The T_{m02} during monsoon varied from 3.4 to 9.7 s with an average value of 6.2 s (Figure 2b) and the peak wave period (T_p) ranged from 3.8 to 20 s with an average value of 10.5 s (Figure 2c). From February to May (pre-monsoon), waves from northwest (wave direction > 248°) were observed (Figure 2d) and are predominant for 19.4% of time (Figure 3). These waves had a H_s ranging from 0.25 to 2.86 m, T_{m02} ranging from 4.5 to 8.5 s and T_p ranging from 2.2 to 22.2 s. During the post-monsoon season (October–January) waves mostly approach from the southwest (Figure 3) with H_s varying from 0.2 m to 2.5 m, T_{m02} from 2.5–9.6 s

and T_p from 2.1–22.2 s. This seasonal distribution of waves indicates that study the region has 3 wave regimes: (i) swells (T_p > 10 s) from the southwest, (ii) wind-seas (H_s < 1.5 m & T_p < 8 s) from the northwest and (iii) westerly waves during monsoon (H_s > 1.5 m) (Figure 3).

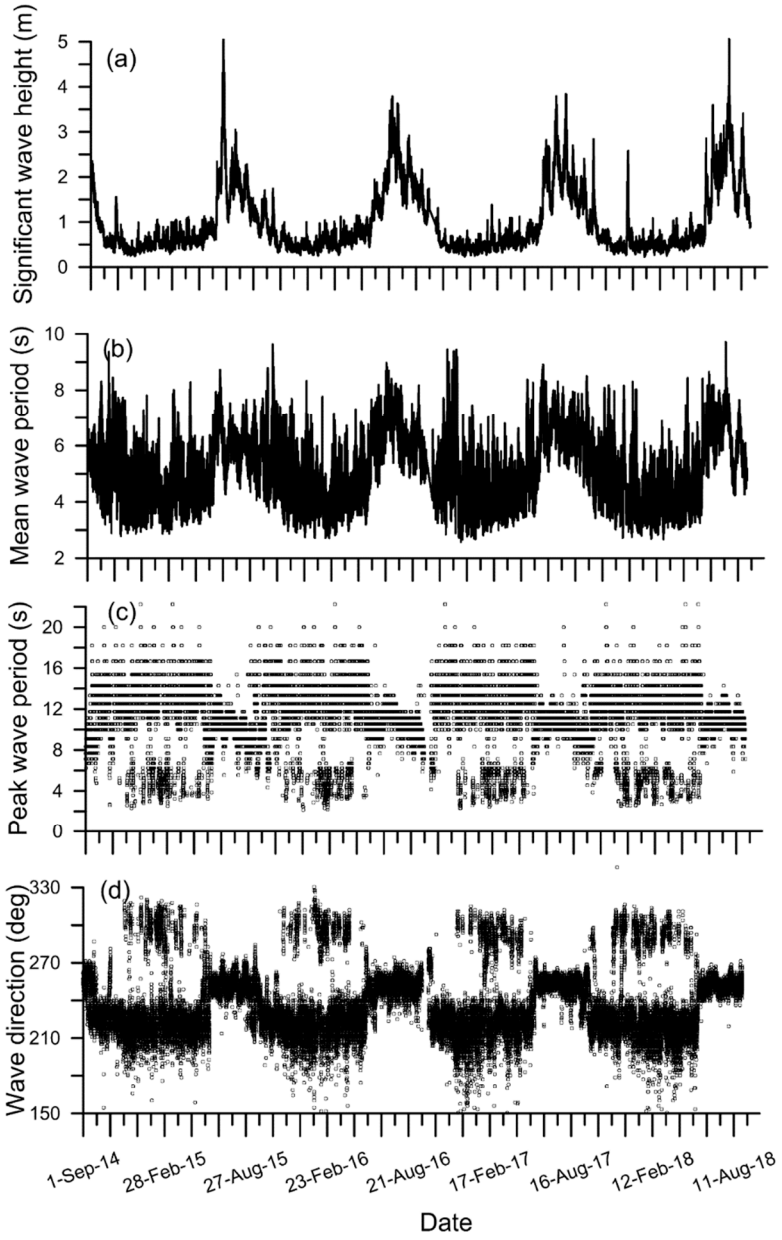

Figure 2. Time series plot of (**a**) significant wave height, (**b**) mean wave period, (**c**) peak wave period and (**d**) mean wave direction from 1 September 2014 to 31 August 2018 at 15 m water depth.

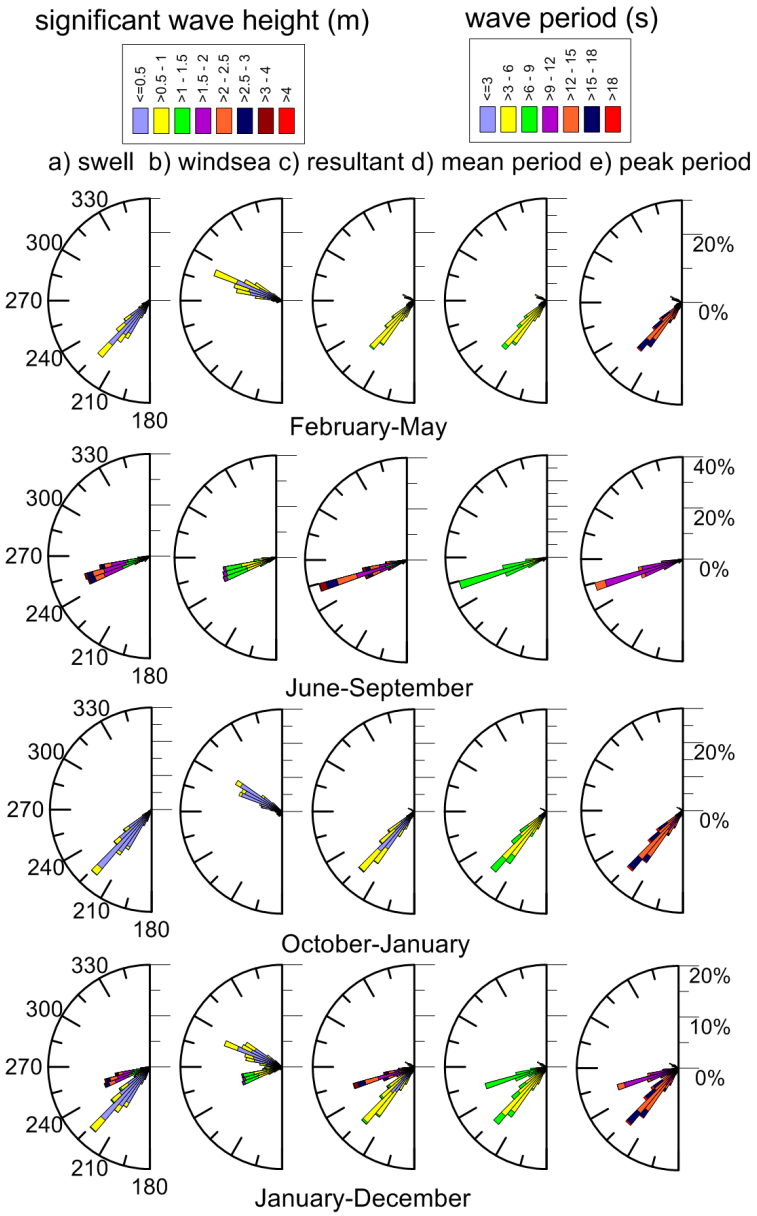

Figure 3. Wave rose diagram for significant wave height of (**a**) swell, (**b**) wind-sea and (**c**) resultant. The right panel is for (**d**) mean wave period and (**e**) peak wave period in different seasons from 1 September 2014 to 31 August 2018 at 15 m water depth.

The highest H_s of about 2 m along the study region during non-monsoon months was previously reported by Amrutha et al. [25] and the existence of long-period waves (T_p > 18 s) along the eastern Arabian sea was also previously reported [49,50]. T_{m02} values observed off Vengurla are similar to the value (7–8 s) observed off the Goa coast [46]. During the study period, 71% of the waves had a H_s less than 1 m and 2% of the waves had a H_s of more than 3m. The annual average values of H_s during the four-yearly cycles (2014–2015, 2015–2016, 2016–2017, 2017–2018) are 0.94, 1.02, 0.95 and 1.01 respectively, indicating an inter-annual variation of up to 8%. However, no significant variations in annually averaged values of T_{m02} (5.1, 5.3, 5.3 and 5.1 s) and T_p (11.6, 11.8, 11.6 and 11.3 s.) were observed during different annual cycles.

The surface height variance at the study area is separated into wind-seas and swells (see data and methodology) and the resulting wave height, mean wave period and wave direction of wind-seas and swells for different months during different annual cycles are presented in Tables 2 and 3, respectively. The monthly average swell H_s varies from 0.24 to 2.23 m, whereas the monthly averaged wind-sea H_s

varies from 0.21 to 1.17 m. The wave period and direction for both wind-sea and swells are observed to be somehow consistent, and their variation is observed to be less than 3% annually for different months. Most importantly, the wind-sea H_s is comparable to swell H_s during non-monsoon seasons (Tables 2 and 3).

During most of the time, the wave spectrum in the study area consisted of multiple peaks, except in the monsoon season which had considerable energy in the secondary peak (Figure 4). The wave direction corresponding to both the primary and the secondary peak was also different. Hence, the spectral energy density at the primary peak and the secondary peak are compared separately for the monsoon and non-monsoon period (Figure 5). At both water depths (15 and 5 m) during the monsoon, the spectral energy density at secondary peak is ~40% of that in the primary peak. During the non-monsoon period, the energy at the secondary peak is 49% (28%) of that in the primary peak at 15 m (5 m) water depth. There is a significant difference between the direction of the wind-sea and the swells, especially during the non-monsoon months at both 15 m and 5 m water depth (Figure 4).

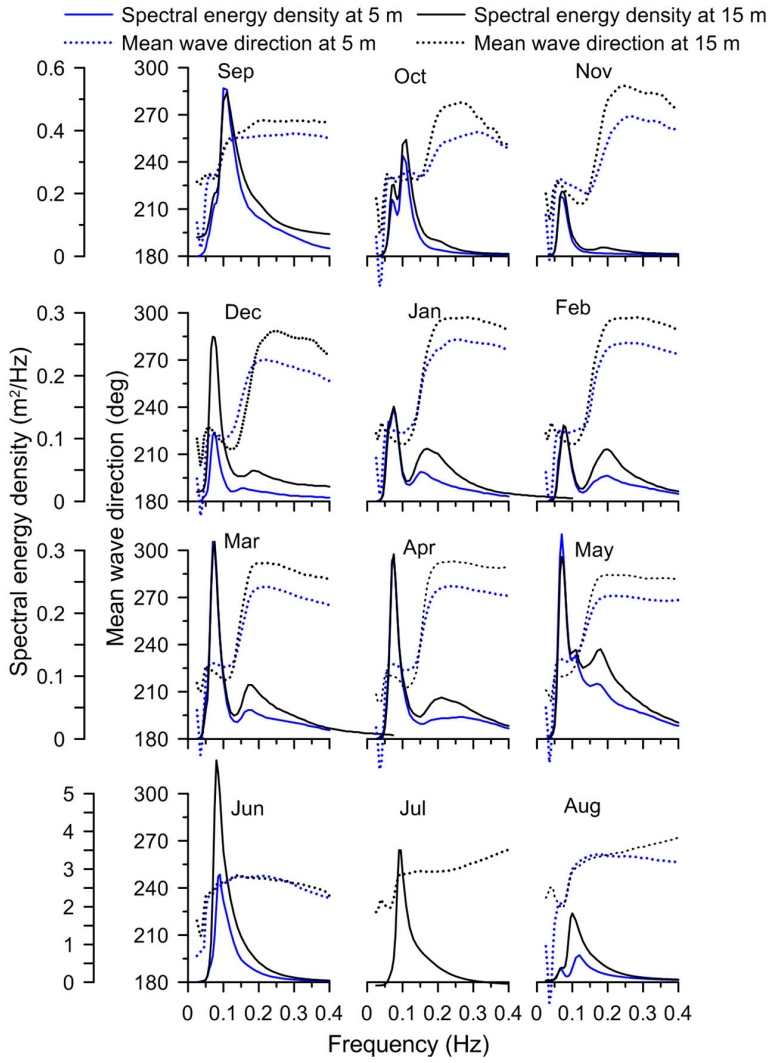

Figure 4. Monthly averaged wave spectrum showing the variation of spectral energy density and mean wave direction at both 15 and 5 m water depth.

Table 2. Monthly average of significant wave height, mean wave period and mean wave direction of swell measured at 15 m water depth for four years.

Month	Swell											
	H_s (m)				Wave Period (s)				Direction (deg)			
	2014–2015	2015–2016	2016–2017	2017–2018	2014–2015	2015–2016	2016–2017	2017–2018	2014–2015	2015–2016	2016–2017	2017–2018
Sep.	1.01	0.80	1.13	0.88	8.8	9.4	8.8	8.8	245	237	249	242
Oct.	0.52	0.50	0.39	0.42	10.0	10.6	10.4	10.2	229	224	225	223
Nov.	0.35	0.37	0.39	0.28	11.1	10.5	11.6	11.0	223	223	222	221
Dec.	0.27	0.28	0.25	0.45	10.8	10.9	11.1	10.8	219	219	212	225
Jan.	0.32	0.28	0.27	0.24	11.6	11.7	11.5	11.0	225	216	219	218
Feb.	0.27	0.26	0.32	0.26	11.1	10.6	10.4	11.5	223	224	224	215
Mar.	0.41	0.35	0.32	0.31	11.5	11.9	11.7	10.9	224	224	225	219
Apr.	0.40	0.46	0.34	0.38	11.1	11.1	10.8	11.1	221	223	221	216
May	0.47	0.89	0.71	0.69	10.7	10.0	10.5	10.0	225	235	230	226
Jun.	1.80	1.78	1.90	1.79	9.3	9.5	9.4	9.2	245	249	253	251
Jul.	1.54	2.0	1.87	2.23	8.9	9.6	9.4	9.7	252	251	253	250
Aug.	1.18	1.60	1.42	1.43	8.8	8.7	8.9	8.8	250	252	250	253

Table 3. Monthly average of significant wave height, mean wave period and mean wave direction of wind-sea measured at 15 m water depth for four years.

Month	Wind-Sea											
	H_s (m)				Wave Period (s)				Direction (deg)			
	2014–2015	2015–2016	2016–2017	2017–2018	2014–2015	2015–2016	2016–2017	2017–2018	2014–2015	2015–2016	2016–2017	2017–2018
Sep.	0.71	0.57	0.74	0.57	3.7	3.8	3.8	3.7	263	265	256	263
Oct.	0.31	0.39	0.44	0.38	3.4	3.5	3.7	3.6	265	244	283	261
Nov.	0.25	0.31	0.21	0.29	3.1	3.4	3.1	3.4	279	261	285	292
Dec.	0.32	0.34	0.29	0.42	3.3	3.3	3.3	3.4	274	278	278	266
Jan.	0.42	0.36	0.34	0.40	3.5	3.4	3.3	3.5	295	291	293	293
Feb.	0.43	0.49	0.42	0.36	3.4	3.4	3.4	3.4	294	292	282	288
Mar.	0.44	0.46	0.48	0.44	3.4	3.4	3.5	3.4	291	289	290	284
Apr.	0.44	0.55	0.46	0.42	3.2	3.4	3.4	3.2	292	291	283	289
May	0.57	0.63	0.52	0.57	3.5	3.4	3.4	3.4	283	273	273	270
Jun.	1.02	0.93	0.96	0.93	3.8	3.9	4.0	3.9	246	254	250	251
Jul.	1.02	1.03	1.01	1.17	3.7	4.01	3.9	3.9	253	252	251	250
Aug.	0.82	0.95	0.77	0.98	3.9	3.7	3.9	3.7	260	252	256	254

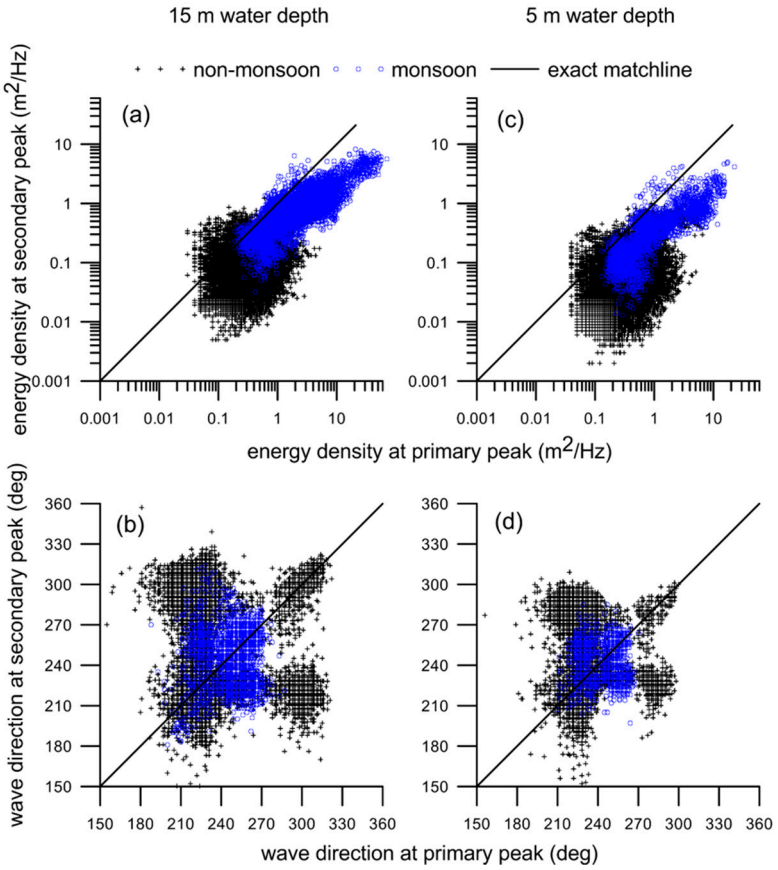

Figure 5. Top panel shows the scatter plot of spectral energy density at secondary peak with primary peak. Bottom panel shows the scatter plot of the wave direction at primary peak and secondary peak. The wave data from September 2014 to August 2015 at 15 m water depth is presented in (**a**,**b**) and that at 5 m water depth in (**c**,**d**).

4.2. Model Validation and Comparison

The performance of the Delft-3D WAVE module is assessed by comparing the model results with the measured data at 5 m water depth from September 2014 to June 2015 and August 2015. The output parameters from the numerical wave model which are used as input to the LSTR estimate are significant wave height, peak wave period and wave direction. Hence, these parameters are compared with the measured buoy data at 5 m water depth. The skill of the model is determined based on the amount of deviation which is measured by root-mean-square error (RMSE) and bias between the model results and the observational data and the correlation coefficient (R). The comparison of the measured and simulated wave parameters at 5 m water depth for both non-monsoon and monsoon seasons are presented in Figure 6. During non-monsoon season, H_s shows a bias of −0.012 m, RMSE of 0.063 m and the correlation coefficient (R) is 0.93. On the other hand, the bias, RMSE and R values of the mean wave period (T_{m02}) and wave direction during non-monsoon are −1.26 s, 1.55 s, 0.73 and 3.7°, 19.7°, 0.44 respectively. During monsoon, the bias, RMSE and R values for H_s are 0.041 m, 0.22 m, and 0.91 respectively and for T_{m02} and wave direction, the values are −0.77 s, 1.03 s, 0.77 and −0.06°, 9.42°, 0.65 respectively. It is observed that both H_s and T_{m02} underpredicts by ~18% during monsoon season, and by 16% and 23% during non-monsoon, whereas the direction underpredicts less than 2% during both seasons. During the non-monsoon period, when the wind-sea is stronger and close to the swell energy, the comparison between the wave direction between the model and the measured data show large scatter. The performance of the model using the separated swell and wind-sea has also been compared with the measured data (Figure 6) and is presented in Table 4. Kumar et al. [21] observed

that the Delft-3D wave module [17] results are comparable (RMSE ~0.067 m, bias ~0.017 m and SI ~0.083) with the measured data at a water depth of 2.5 m.

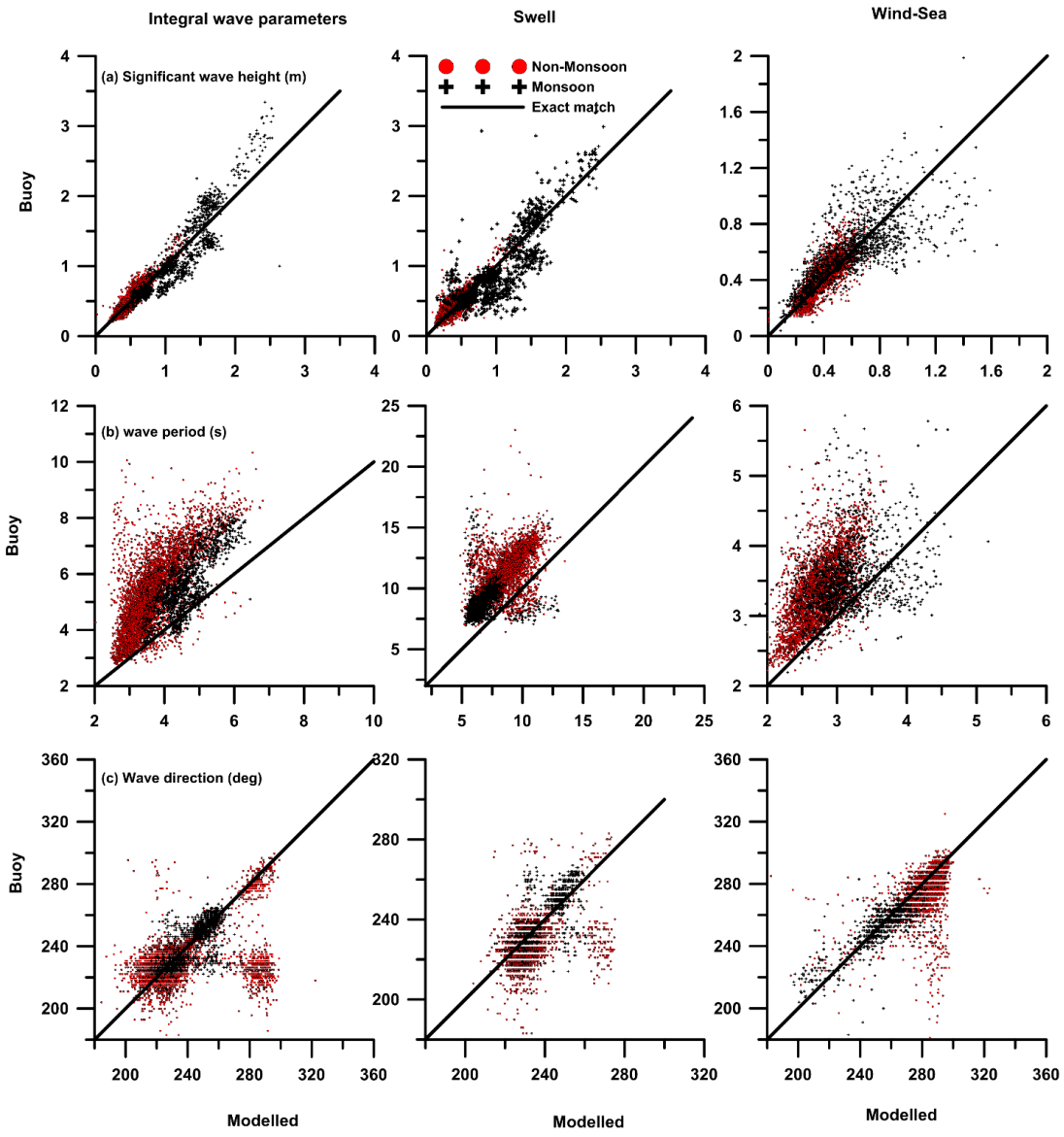

Figure 6. Scatter plot of (**a**) significant wave height, (**b**) mean wave period and (**c**) mean wave direction for integral wave parameters, swell and wind-sea between measured buoy data at 5 m water depth and that based on wave model.

4.3. Breaker Characteristics

During the post-monsoon season, breaker heights (H_b) less than 1 m are observed (Figure 7a). Along the study region, Chandramohan et al. [51] observed breaker heights of about 0.7 m and mean wave periods of 5–8 s during non-monsoon seasons. There is a considerable increase in the wave height to about 2 m during the monsoon with its peak around 3.8 m during 2015 (Figure 7a). During the study period, about 69% of the wave height is less than or equal to 1 m and during 17% of the time, H_b exceeded 1.5 m (Figure 7a). Off the central west coast of India, Shanas and Kumar [4] observed that during an annual cycle, 0.6–1.1 m waves occurred for about 55% of the time. Wave period at the breaker zone generally varies in the range of 2.7–9.6 s with an average value of 4.4 s. (Figure 7b). Also, Figure 7c clearly shows that the breaker angle decreased during the monsoon period and is high during the non-monsoon season. The frequency distribution indicates that around 19% of waves break

at angles of more than 20° and 44% of waves break at an angle less than 10°. About 74% of the time, breaker angle is directed towards the north. The predominance of northerly directed waves in the eastern Arabian Sea were previously reported by Jesbin et al. [42].

Table 4. Statistical comparison of swell and wind-sea parameters between measured and model data during monsoon and non-monsoon.

Season	Swell								
	Hs (m)			Mean Wave Period (s)			Direction (deg)		
	Bias	RMSE	R	Bias	RMSE	R	Bias	RMSE	R
Monsoon	0.08	0.28	0.84	−2	2.6	0.2	−1.7	10.2	0.55
Non-Monsoon	−0.02	0.07	0.9	−2.7	3.01	0.58	4.5	10.4	0.42
	Wind-Sea								
	Hs (m)			Mean Wave Period (s)			Direction (deg)		
	Bias	RMSE	R	Bias	RMSE	R	Bias	RMSE	R
Monsoon	0.01	0.19	0.72	−0.38	0.69	0.31	3	12.1	0.73
Non-Monsoon	0.006	0.06	0.87	−0.63	0.75	0.58	8.2	22.1	0.55

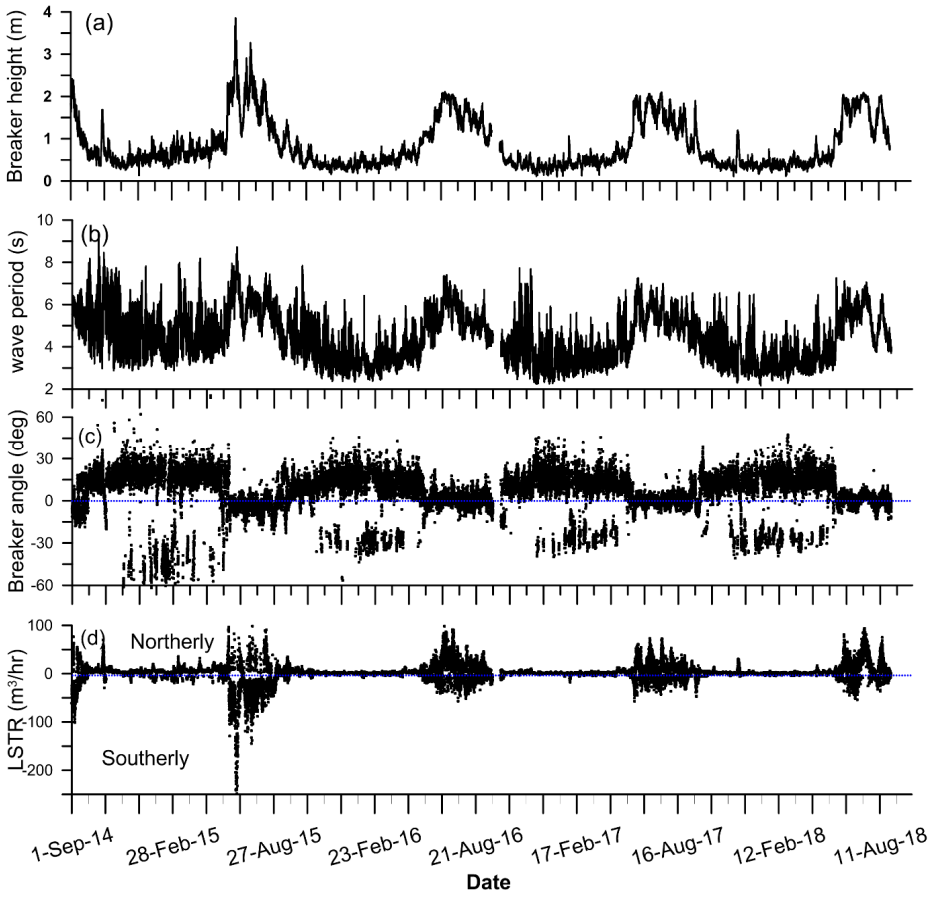

Figure 7. Time series plot for (**a**) breaker height, (**b**) wave period (**c**) wave breaker angle, and (**d**) longshore sediment transport rate.

4.4. LSTR Estimate Based on Integral Wave Parameters

LST rates along the Vengurla coast during different months of four annual cycles were estimated using Equation (1). Estimated LSTR is low during the non-monsoon period due to small breaker

heights (Table 5). The annual gross LSTR ranges from 0.59–0.74 × 10^5 m^3/yr for the study region. The gross LSTR for a region ~140 km north of the study area is 0.4 × 10^5 m^3/yr [26]. Shanas and Kumar [4] and Kumar et al. [21] along the Kundapura and Malpe coasts estimated LST using the Kamphuis equation and reported an LSTR of 1.63 × 10^5 m^3/yr and 8.9 × 10^5 m^3/yr, respectively, indicating that there are large variations in the gross LSTR within a 440 km stretch along the central west coast of India. Chandramohan and Nayak [52] have reported that the south Maharashtra coast has a negligible annual net LSTR. The monthly pattern shows that net LSTR varied from 13 (in February) to 19,993 (in June) m^3/month (Table 5). Previously, along the study region, based on visual observations of breaker heights and period, Chandramohan et al. [51] estimated a southerly directed net LSTR of 0.53 × 10^5 m^3/yr. Recently, Noujas et al. [27], using a LITDRIFT model, estimated the LSTR of 1.18 × 10^5 m^3/yr along Vengurla coast with an annual net value ranging from −7778 to −9015 m^3/yr. The annual net value for the present study is observed to be ranging from 0.26 to 0.37 × 10^5 m^3/yr, and the transport is towards the north. The direction of sediment transport is predominantly towards the north from June to September (Figure 7d) which is due to the predominance of southwesterly swell waves (Figure 3) along this region. However, large southerly LST rates were observed during the 2015 monsoon, which was associated with high breaker heights (Figure 7a) and southerly breaker heights (Figure 7c). During the pre-monsoon, sediment transport was predominantly observed to be southerly with low magnitude. The longshore current is responsible for the directional change during the monsoon, and the seasonal wind pattern is responsible for the change in the direction of LSTR during non-monsoon.

Table 5. Monthly net and gross longshore sediment transport rate using the measured buoy data for four years.

Month	LSTR Based on Buoy Data							
	Gross (m^3/month)				Net (m^3/month)			
	2014–2015	2015–2016	2016–2017	2017–2018	2014–2015	2015–2016	2016–2017	2017–2018
Sep.	8294	5835	5169 *	6077	319	3638	1615 *	−380
Oct.	2773	3060	2092*	2253	1411	2857	395 *	1967
Nov.	1409	1698	1845	1094	1357	1393	1835	735
Dec.	988	1144	880	2893	735	735	880	2301
Jan.	1558	1029	964	994	632	803	578	347
Feb.	1134	1336	1521	861	13	−263	−297	465
Mar.	2280	1600	1485	1414	1441	1152	609	755
Apr.	1925	2621	1696	1790	1500	1664	624	1585
May	2643	5313	4331	3258	1827	−475	1585	1009
Jun.	19,407	17,309	16,160	14,798	15,510	11,444	5842	6283
Jul.	12,182	19,670	13,519	24,256	1380	12,104	2518	19,993
Aug.	10,747	13,577	10,290	10,644	113	−2432	3450	2635
Annual	65,340	74,192	59,952	70,332	26,238	32,620	19,634	37,695

* In 2015–2016 LSTR estimate in September is based on 20 days and October is 26 days.

Variation of LSTR with the H_s indicates that the LST increases with an increase in the wave height and decreases with the reduction of wave height (Figure 8). LST rates are influenced mainly by the breaker parameters [14]. The influence of breaker height on LSTR for different seasons is studied through a scatter plot between these two parameters during the annual cycle 2014–2015 (Figure 8). The breaker height is high during the monsoon and is in the order of 1 to 2 m; the LSTR is also high during this season. Wave breaker angle is low during the monsoon, whereas the sediment transport is

high during this time (Figure 8). Noujas et al. [27] examined the sensitivity analysis of net LSTR by increasing the wave height contribution by 10% and observed an increasing trend in LSTR. Recently, Jesbin et al. [26] investigated the influence on variations in LSTR due to errors in breaking angle and breaker height and observed that they are sensitive to LST rates and could lead to large errors in their estimation. There is a high variability of LSTR during the monsoon season. The annual gross LST for 5%, 10%, 15% and 20% increases in the H_s values are 71,933, 78,961, 86,427 and 94,322 m^3/yr. A 5%, 10%, 15% and 20% increases in the H_s value results in 10%, 21%, 32% and 44% increases in the annual LST. Even though the waves are influenced by the sea breeze during the pre-monsoon period, the influence of sea breeze on LST is negligible (figure not shown) since the LST depends on both the wave height and wave period and these two parameters have an inverse relationship during the sea breeze period [49,53].

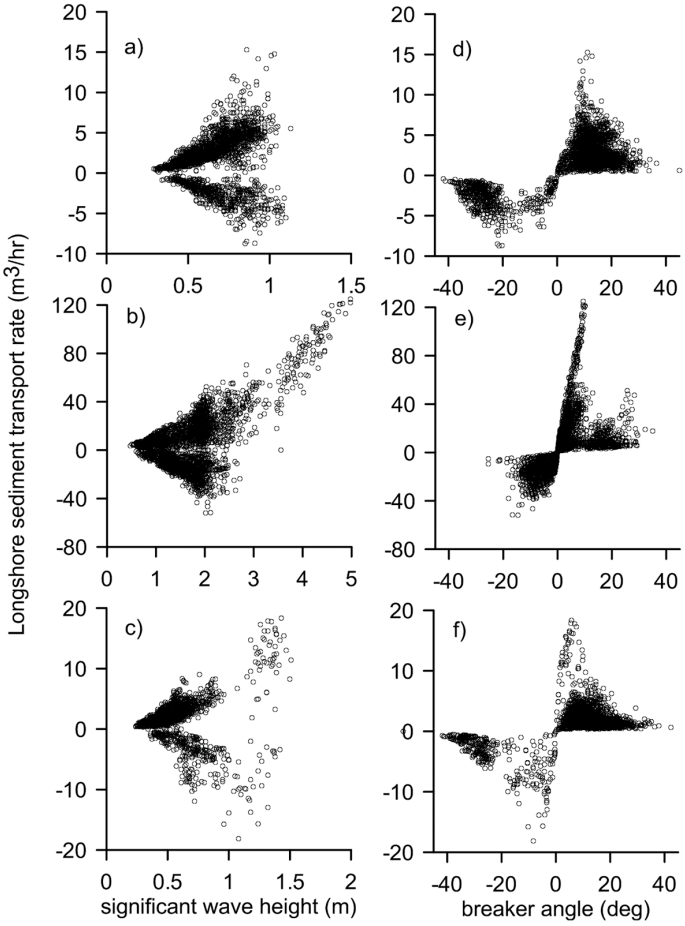

Figure 8. Influence of wave breaker height on the LSTR (**a**–**c**) and wave breaker angle on LSTR (**d**–**f**) in different seasons from September 2014 to August 2015. (**a**,**d**) pre-monsoon (February–May), (**b**,**e**) monsoon (June–September) and (**c**,**f**) post-monsoon (October–January).

4.5. LSTR Estimate Based on Wind-Sea and Swells

As discussed in Section 4.1, wind-seas and swells along the study region are comparable during non-monsoonal months. Thus, LSTR based on the separated wind-seas and swells were estimated along the study region from September 2014 to August 2015 (Table 6). Monthly gross LSTR based on wind-sea varies from 244 m^3/month (in November) to 3232 m^3/month (in June), whereas that based on swell varies from 1461 m^3/month (in February) to 23,018 m^3/month (in June). The wind-sea contribution to the monthly gross LSTR varies from 6% to 25% with the lowest in March and the highest in June. The bulk (75% to 94%) of the gross LSTR is due to swells (Table 6). Based on remote sensing

techniques, Kunte and Wagle [54] reported that sediment transport direction along the Maharashtra coast is bidirectional and seasonal-dependent.

Table 6. Monthly net and gross longshore sediment transport rate using the measured buoy data separated into wind-sea and swell and ERA-Interim data.

Month	LSTR Using ERA-Interim Data		LSTR Due to Wind-Sea		LSTR Due to Swell		Total LSTR	
	Gross (m^3/month)	Net (m^3/month)	Gross (m^3/month)	Net (m^3/month)	Gross (m^3/month)	Net (m^3/month)	Gross (m^3/month)	Net (m^3/month)
Sep 2014	15,178	6447	1813	−1503	10,671	2664	12,485	1160
Oct 2014	15,699	15,699	425	−142	4539	2958	4965	2816
Nov 2014	8179	6437	244	−194	3576	3556	3821	3362
Dec 2014	5120	1553	399	−346	2011	1858	2411	1512
Jan 2015	5615	−2419	716	−711	2911	2394	3627	1683
Feb 2015	4027	446	615	−606	1810	1461	2425	854
Mar 2015	10,050	6011	762	−683	5114	4313	5876	3629
Apr 2015	10,976	8816	657	−622	4402	4106	5060	3483
May 2015	7873	4621	1278	−1257	5044	3958	6323	2700
Jun 2015	29,741	28,918	3232	1369	27,131	23,018	30,363	24,387
July 2015	27,564	−21,481	2291	−1269	18,432	6619	20,723	5323
Aug 2015	16,447	−9353	2468	−1956	13,085	4124	15,553	2168
Annual	156,469	45,695	14,900	−7920	98,726	61,029	113,632	53,077

From Table 6, it is evident that wind-seas generally contribute to the southerly net transport of LST, whereas swells contribute to northerly net LST. The annual gross LSTR due to wind-seas is 0.149×10^5 m^3 and that due to swells is 0.987×10^5 m^3. The annual gross LSTR based on bulk wave parameters (0.6534×10^5 m^3/yr) is only 58% of that considering the wind-seas and swells (1.13632×10^5 m^3/yr). The gross transport during the pre-monsoon, monsoon and post-monsoon period is 13%, 70% and 17% of the annual transport. Similarly, the net transport during the pre-monsoon, monsoon and post-monsoon period is 10%, 78% and 12%. The LSTR based on integral wave parameters is less (37% to 47%) based on relative contribution of wind-seas and swells during November to May, when both wind-seas and swells coexist in the area. During monsoon, when swells dominate, the LSTR based on integral wave parameters is 64% to 66% of that based on relative contribution of wind-seas and swells. For incoming west–southwesterly wave conditions, which are predominantly swells, the LSTR is generally higher due to higher spectral peak periods and higher significant wave height (Figure 8e). For incoming north-westerly waves, which are predominantly wind-seas, the LSTR is lower due to lower wave periods and lower significant wave heights. The study shows that in regions where there is a large difference in the direction of the wind-seas and swells, considering the integral parameters will lead to errors in the LSTR estimate. Studies of this type, involving model calibration based on field measurements, considering relative contribution of wind-seas and swells, are deemed to provide a useful perspective on the LSTR to be applied for coastal engineering applications and morphological studies.

4.6. LSTR Estimate Based on ERA-Interim Data

In most of the locations, the measured wave data is not available. Thus, the researchers use reanalysis data, such as ERA-Interim or ERA-40 [55] produced by the European Centre for Medium Weather Forecasts, for estimation of the LSTR. Many researchers across the globe have used these datasets to estimate LST rates [42,56] and to understand the physical mechanism driving the wave climate [57]. For example, temporal variations in annual net LST rates were examined using ERA datasets in southeast Queensland, Australia and were linked to climate indices [56]. Along the west

coast of India, Jesbin et al. [42] and Chowdhury et al. [58] estimated temporal variations in LST using ERA datasets and established a link with pacific climate variability and the latitudinal position of the inter-tropical convergence zone (ITCZ), respectively. Hence, we have compared the LSTR estimate based on ERA-Interim with the buoy-measured wave data. The monthly gross and net LSTR shows a large difference in the LSTR estimate based on ERA-Interim data compared (Table 6) to that based on measured buoy data (Table 5).

The large difference in the LSTR between the two estimations is due to the large difference in the wave period and wave direction between the two datasets (Figure 9). Breaker height from ERA-Interim H_s can be estimated with an RMSE of 0.29 m for the study area, but the wave direction shows large scatter (up to 17°) (Figure 9). Even a 20% increase in the H_s value results in a 44% increase in the annual LST [24]. An earlier study [59] showed that the ERA-Interim wave period is close to the energy wave period ($T_e = m_{-1}/m_0$) and not the mean wave period of the buoy data and hence, there is large scatter between the mean wave period of the buoy-measured data and the ERA-Interim data (Figure 9). The large difference in the wave direction is due to the fact that ERA-Interim data is based on a low-resolution global model (0.70° for the atmospheric model and 1° for the ocean model [43]) and also the measurements are made in the nearshore environment. Another reason for the substantial difference between the wave direction of the ERA-Interim and the buoy data is due to the predominance of wind-seas and swells in the study area. During the non-monsoon period, in some of the instances, the spectral energy of the wind-sea peak and the swell peak have comparable energy, and during this period, the direction of the wind-sea and swell have a large difference (Figure 5). In some cases, the ERA-Interim data shows the swell direction, whereas the measured data represent the wind-sea direction, whereas, in other instances, vice versa is observed (Figure 10). Also, the short-term sub-synoptic scale wind pulses and fluctuations are not likely to be captured by a lower resolution ERA-Interim data [42,59]. Hence, datasets like ERA-Interim cannot be solely used for studying the nearshore processes, especially for estimating the LSTR without validation.

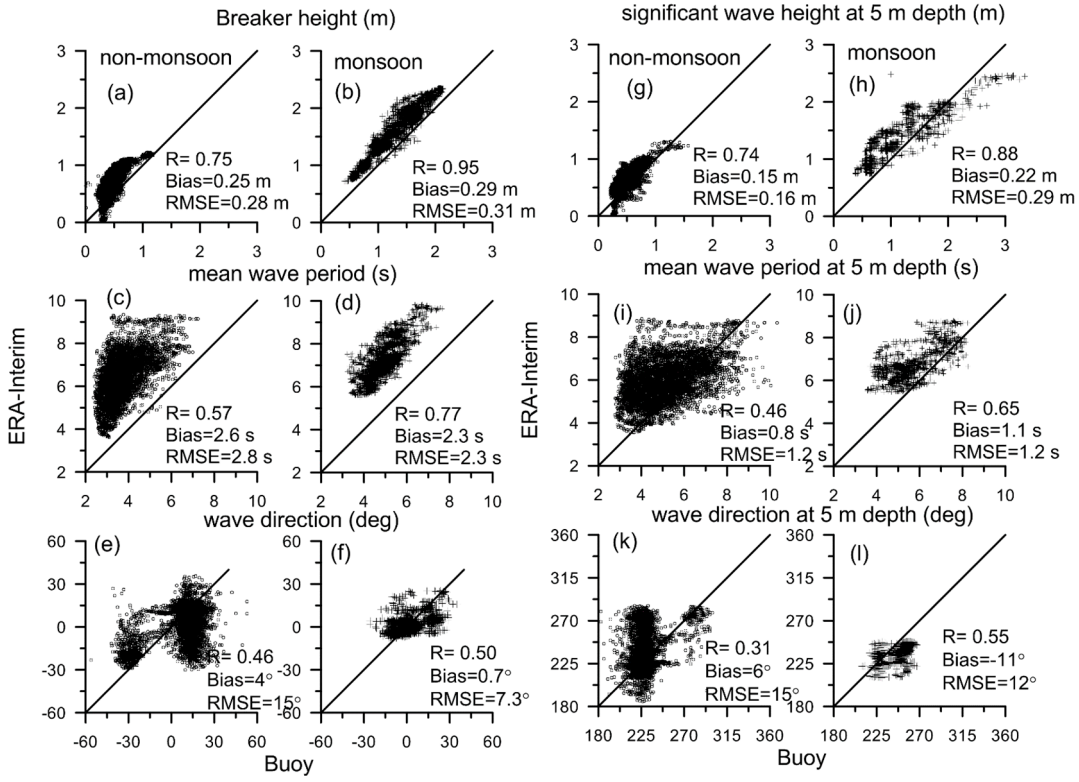

Figure 9. (**a**–**f**) Scatter plot between the breaker parameters from buoy-measured data and ERA-Interim data. (**g**–**l**) Scatter plot between buoy-measured data and ERA-Interim data at 5 m water depth.

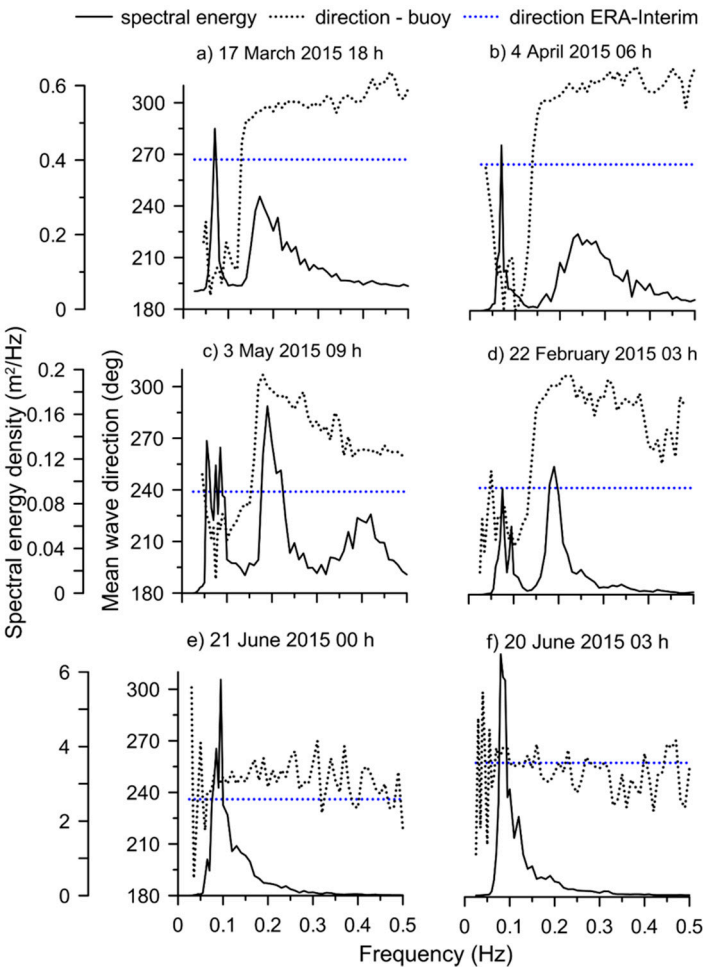

Figure 10. Plots showing the wave spectral energy density and mean wave direction from measured buoy data during different wave conditions along with ERA-Interim wave direction. (**a**,**b**) are swell-dominated multi-peaked wave spectra, (**c**,**d**) are wind-sea dominated multi-peaked wave spectra, and (**e**,**f**) are single-peaked spectra during the monsoon.

5. Conclusions

The present study examines the wave characteristics and longshore sediment transport rate (LSTR) for four different annual cycles along the Vengurla coast. The wave data collected at a 15 m water depth at 1 h intervals is used, and the nearshore wave parameters are estimated using a numerical model Delft 3D Wave model. The results have been compared with field-measured data from a buoy, and thus derived parameters are employed for estimating the LSTR. The model results show good agreement with the measured data. Annually, Hs is observed to be varying up to 8%, whereas the mean wave period and peak wave period show no significant inter-annual variations. The study area has three wave regimes: swells from the southwest, wind-seas from the northwest and westerly waves during the monsoon, with comparable wind-seas and swells. Gross LSTR along the region is high during monsoon and non-monsoon periods, LSTR is of low magnitude and varies annually in the range of 0.59–0.74 $\times 10^5$ m^3/yr. LST direction depends on the breaker direction and is predominantly northward, and hence the monthly net LSTR is towards the north in all months, but the estimate based on ERA-Interim reanalysis data produce a southerly LST in January, July and August. A small error in the breaker angle induces larger errors in the LSTR and, hence, for studies based on LSTR estimation, lower-resolution datasets like ERA-Interim should be used only after validation with measured data, especially in the regions where comparable wind-seas and swells exist. The studies indicate that there is a large variation in the gross LSTR within a 440 km stretch along the central west

coast of India. In this study, the relative contribution of wind-seas and swells on LSTR are specifically examined. All previous studies have focused on the integral wave parameters of the wind-seas and swells. The annual gross LSTR based on integral wave parameters is only 58% of that considering the wind-seas and swells separately. In regions where there is large difference in the direction of the wind-seas and swells, considering the integral parameters will lead to errors in the LSTR estimate.

Author Contributions: Conceptualization, J.G. and V.S.K.; methodology, J.G.; formal analysis, J.G.; resources, R.G. and J.S.; writing—original draft preparation, J.G.; writing—review and editing, V.S.K.; supervision, V.S.K.; All authors have read and agreed to the published version of the manuscript.

Funding: This research received no external funding

Acknowledgments: The authors gratefully acknowledge the support of the Council of Scientific & Industrial Research, New Delhi to conduct this research. The ERA-I data used in this study are available from the ECMWF data server https://apps.ecmwf.int/datasets/data/interim-full-daily/levtype=sfc/. The wave data used for the model validation are from the project funded by Earth System Science Organization, Ministry of Earth Sciences, Government of India and are available on request for joint research work. Director, CSIR-NIO, Goa encouraged us to carry out the study. We thank Jai Singh, P.R.Shanas, T.R.Anoop, Naseef Muhammad for the help provided during the data collection. We thank the three reviewers for the suggestions which improved the scientific content of this paper. This work forms part of the Ph.D. thesis of the first author registered at Bharathidasan University and NIO contribution No. is 6493.

Conflicts of Interest: The authors declare no conflict of interest.

References

1. Dean, R.G.; Dalrymple, R.A. *Coastal Processes—With Engineering Applications*; Cambridge University Press: Cambridge, UK, 2002. [CrossRef]
2. Zhang, S.; Jia, Y.; Zhang, Y.; Shan, H. Influence of seepage flows on the erodibility of fluidized silty sediments: Parameterization and mechanisms. *J. Geophys. Res. Ocean* **2018**. [CrossRef]
3. Pilkey, O.H.; Cooper, J.A.G. Are natural beaches facing extinction? *J. Coast. Res.* **2014**, *70*, 431–436. [CrossRef]
4. Shanas, P.R.; Sanil Kumar, V. Coastal processes and longshore sediment transport along Kundapura coast, central west coast of India. *Geomorphology* **2014**, *214*, 436–451. [CrossRef]
5. Bergillos, R.J.; Rodríguez-Delgado, C.; Ortega-Sánchez, M. Advances in management tools for modeling artificial nourishments in mixed beaches. *J. Mar. Syst.* **2017**, *172*, 1–13. [CrossRef]
6. Bergillos, R.J.; López-Ruiz, A.; Principal-Gómez, D.; Ortega-Sánchez, M. An integrated methodology to forecast the efficiency of nourishment strategies in eroding deltas. *Sci. Total Environ.* **2018**, *613–614*, 1175–1184. [CrossRef]
7. López-Ruiz, A.; Solari, S.; Ortega-Sánchez, M.; Losada, M. A simple approximation for wave refraction—Application to the assessment of the nearshore wave directionality. *Ocean Model.* **2015**, *96*, 324–333. [CrossRef]
8. Bergillos, R.J.; López-Ruiz, A.; Ortega-Sánchez, M.; Masselink, G.; Losada, M.A. Implications of delta retreat on wave propagation and longshore sediment transport—Guadalfeo case study (southern Spain). *Mar. Geol.* **2016**, *382*, 1–16. [CrossRef]
9. Bergillos, R.J.; Masselink, G.; Ortega-Sánchez, M. Coupling cross-shore and longshore sediment transport to model storm response along a mixed sand-gravel coast under varying wave directions. *Coast. Eng.* **2017**, *129*, 93–104. [CrossRef]
10. Watt, G.M. *A Study of Sand Movement at South Lake Worth Inlet, Florida*; No. TM-42; Coastal Engineering Research Center: Vicksburg, MS, USA, 1953.
11. Caldwell, J.M. *Wave Action and Sand Transport near Anheim Bay, California*; No. TM-68; U.S. Beach Erosion Board: Washington, DC, USA, 1956.
12. Ingle, J.C., Jr. *The Movement of Beach Sand, Developments in Sedimentology*; Cambridge University Press: Cambridge, UK, 1966.
13. Komar, P.D.; Inman, D.L. Longshore sand transport on beaches. *J. Geophys. Res.* **1970**, *75*, 5914–5927. [CrossRef]
14. Smith, E.R.; Wang, P.; Ebersole, B.A.; Zhang, J. Dependence of Total Longshore Sediment Transport Rates on Incident Wave Parameters and Breaker Type. *J. Coast. Res.* **2009**, *253*, 675–683. [CrossRef]

15. USACE. *Shore Protection Manual*; Coastal Engineering Research Center (CERC): Washington, DC, USA; U.S. Government Printing Office: Vicksburg, MS, USA, 1984; Volume I–II.
16. Chempalayil, S.P.; Kumar, V.S.; Dora, G.U.; Johnson, G. Near shore waves, long-shore currents and sediment transport along micro-tidal beaches, central west coast of India. *Int. J. Sediment Res.* **2014**, *29*, 402–413. [CrossRef]
17. Walton, T.L., Jr.; Bruno, R.O. Longshore Transport at a Detached Breakwater, Phase II. *J. Coast. Res.* **1989**, *5*, 679–691.
18. Kamphuis, J.W. Alongshore transport of sand. In Proceedings of the 28th International Conference on Coastal Engineering, ASCE, Cardiff, Wales, 7–12 July 2002; pp. 2478–2490.
19. Samaras, A.G.; Koutitas, C.G. Comparison of three longshore sediment transport rate formulae in shoreline evolution modeling near stream mouths. *Ocean Eng.* **2014**, *92*, 255–266. [CrossRef]
20. Bayram, A.; Larson, M.; Hanson, H. A new formula for the total longshore sediment transport rate. *Coast. Eng.* **2007**, *54*, 700–710. [CrossRef]
21. Kumar, V.S.; Shanas, P.R.; Dora, G.U.; Glejin, J.; Philip, S. Longshore sediment transport in the surf zone based on different formulae: A case study along the central west coast of India. *J. Coast. Conserv.* **2017**, *21*, 1–13. [CrossRef]
22. Baba, M.; Dattatri, J.; Abraham, S. Ocean wave spectra off Cochin, west coast of India. *Indian J. Mar. Sci.* **1989**, *18*, 106–112.
23. Vethamony, P.; Aboobacker, V.M.; Menon, H.B.; Kumar, K.A.; Cavaleri, L. Superimposition of wind seas on pre-existing swells off Goa coast. *J. Mar. Syst.* **2011**, *87*, 47–54. [CrossRef]
24. Kumar, V.S.; Anand, N.M.; Ashok, K.; Mandal, S. Multipeakedness and Groupiness of Shallow Water Waves Along Indian Coast. *J. Coast. Res.* **2014**, *19*, 1052–1065.
25. Amrutha, M.M.; Sanil Kumar, V.; Sharma, S.; Singh, J.; Gowthaman, R.; Kankara, R.S. Characteristics of shallow water waves off the central west coast of India before, during and after the onset of the Indian summer monsoon. *Ocean Eng.* **2015**, *107*, 259–270. [CrossRef]
26. George, J.; Sanil Kumar, V.; Victor, G.; Gowthaman, R. Variability of the local wave regime and the wave-induced sediment transport along the Ganpatipule coast, eastern Arabian Sea. *Reg. Stud. Mar. Sci.* **2019**, *31*, 100759. [CrossRef]
27. Noujas, V.; Kankara, R.S.; Rasheed, K. Estimation of Longshore Sediment Transport Rate for a Typical Pocket Beach Along West Coast of India. *Mar. Geod.* **2018**. [CrossRef]
28. Dora, G.U.; Kumar, V.S.; Vinayaraj, P.; Philip, C.S.; Johnson, G. Quantitative estimation of sediment erosion and accretion processes in a micro-tidal coast. *Int. J. Sediment. Res.* **2014**, *29*, 218–231. [CrossRef]
29. Sanil Kumar, V.; Pathak, K.C.; Pednekar, P.; Raju, N.S.N.; Gowthaman, R. Coastal processes along the Indian coastline. *Curr. Sci.* **2006**, *91*, 530–536.
30. Amrutha, M.M.; Sanil Kumar, V.; Singh, J. Changes in nearshore waves during the active sea/land breeze period off Vengurla, central west coast of India. *Ann. Geophys.* **2016**, *34*, 215–226. [CrossRef]
31. Gawali, P.B.; Basavaiah, N.; Hanamgond, P.T. Mineral Magnetic Properties of Sediments of Beaches, Redi–Vengurla Coast, Central West Coast of India: A Seasonal Characterization and Provenance Study. *J. Coast. Res.* **2010**, *263*, 569–579. [CrossRef]
32. Herlekar, M.A.; Sukhtankar, R.K. Morphotectonic studies along the Part of Maharashtra coast, India. *Int. J. Earth Sci. Eng.* **2011**, *4*, 61–83.
33. Davies, L.J. A morphogenic approach to world shorelines. *Z. Geomorphol.* **1964**, *8*, 127–142.
34. Short, A.D. Coastal processes and beaches. *Nat. Educ. Knowl.* **2012**, *3*, 15.
35. Chandramohan, P.; Anand, N.M.; Nayak, B.U. Surfzone dynamics of Konkan coast, India. In *Oceanography of the Indian Ocean*; Oxford and IBH: New Delhi, India, 1992.
36. National Hydrographic Office. *India-West Coast*; National Hydrographic Office: Dehradun, India, 2004.
37. Folk, R.L.; Ward, W.C. Brazos River bar [Texas]; a study in the significance of grain size parameters. *J. Sediment. Res.* **1957**, *27*, 3–26. [CrossRef]
38. Blott, S.J.; Pye, K. Gradistat: A grain size distribution and statistics package for the analysis of unconsolidated sediments. *Earth Surf. Process. Landforms.* **2001**, *26*, 1237–1248. [CrossRef]
39. WL|Delft Hydraulics. *Delft3D User Manual*; Delft Hydraulics: Delft, The Netherlands, 2006.
40. Holthuijsen, L.H.; Booij, N.; Ris, R.C. A spectral wave model for the coastal zone. In *Ocean Wave Measurement and Analysis*; ASCE: New York, NY, USA, 1996; pp. 630–641.

41. López-Ruiz, A.; Bergillos, R.J.; Ortega-Sánchez, M. The importance of wave climate forecasting on the decision-making process for nearshore wave energy exploitation. *Appl. Energy* **2016**, *182*, 191–203. [CrossRef]
42. George, J.; Sanil Kumar, V. Long-term variations in nearshore wave climate and littoral drift at Ganpatipule coast, eastern Arabian Sea and its link to Pacific climate variability. *J. Geophys. Res. C Ocean* **2019**, *124*. [CrossRef]
43. Hasselmann, K.; Barnett, T.B.; Bouws, E.; Carlson, H.; Cartwright, D.E.; Enke, K.; Ewing, J.A.; Gienapp, H.; Hasselmann, D.E.; Kruseman, P.; et al. *Measurements of Wind-Wave Growth and Swell Decay during the Joint North Sea Wave Project (JONSWAP)*; Deutches Hydrographisches Institut: Hamburg, Germany, 1973; pp. 8–12.
44. Battjes, J.A.; Stive, M.J.F. Calibration and verification of a dissipation model for random breaking waves. *J. Geophys. Res. Ocean* **1985**, *90*, 9159–9167. [CrossRef]
45. Eldeberky, Y. Nonlinear transformation of wave spectra in the nearshore zone. *Oceanogr. Lit. Rev.* **1997**, *4*, 297.
46. Portilla, J.; Ocampo-Torres, F.J.; Monbaliu, J. Spectral partitioning and identification of wind sea and swell. *J. Atmos. Ocean. Technol.* **2009**. [CrossRef]
47. Dee, D.P.; Uppala, S.M.; Simmons, A.J.; Berrisford, P.; Poli, P.; Kobayashi, S.; Andrae, U.; Balmaseda, M.A.; Balsamo, G.; Bauer, P.; et al. The ERA-Interim reanalysis: Configuration and performance of the data assimilation system. *Q. J. R. Meteorol. Soc.* **2011**, *137*, 553–597. [CrossRef]
48. Kumar, V.S.; Pednekar, P.; Chandramohan, P.; Kumar, K.; Gowthaman, R. Longshore currents and sediment transport along Kannirajapuram Coast, Tamilnadu, India. *J. Coast. Res.* **2000**, *16*, 247–254.
49. Amrutha, M.M.; Kumar, V.S.; George, J. Observations of long-period waves in the nearshore waters of central west coast of India during the fall inter-monsoon period. *Ocean Eng.* **2017**, *131*, 244–262. [CrossRef]
50. Glejin, J.; Sanil Kumar, V.; Amrutha, M.M.; Singh, J. Characteristics of long-period swells measured in the in the near shore regions of eastern Arabian Sea. *Int. J. Naval Archit. Ocean Eng.* **2016**, *8*, 312–319. [CrossRef]
51. Chandramohan, P.; Sanil Kumar, V.; Nayak, B.U.; Pathak, K. Variation of longshore current and sediment transport along the south Maharashtra coast, west coast of India. *Indian J. Mar. Sci.* **1993**, *22*, 115–118.
52. Chandramohan, P.; Nayak, B.U. Longshore sediment transport model for the Indian west coast. *J. Coast. Res.* **1992**, *8*, 775–787.
53. Anjali Nair, M.; Sanil Kumar, V.; Amrutha, M.M.; Murty, V.S.N. Features of locally and remotely generated surface gravity waves in the inner-shelf region of northwestern Bay of Bengal. *Int. J. Climatol.* **2019**, *39*, 1644–1664. [CrossRef]
54. Kunte, P.D.; Wagle, B.G. Littoral transport studies along west coast of India—A review. *Indian J. Mar. Sci.* **2001**, *30*, 57–64.
55. Uppala, S.M.; Kållberg, P.W.; Simmons, A.J.; Andrae, U.; da Costa Bechtold, V.; Fiorino, M.; Gibson, J.K.; Haseler, J.; Hernandez, A.; Kelly, G.A.; et al. The ERA-40 re-analysis. *Q. J. R. Meteorol. Soc.* **2005**. [CrossRef]
56. Splinter, K.D.; Davidson, M.A.; Golshani, A.; Tomlinson, R. Climate controls on longshore sediment transport. *Cont. Shelf Res.* **2012**, *48*, 146–156. [CrossRef]
57. Harley, M.D.; Turner, I.L.; Short, A.D.; Ranasinghe, R. Interannual variability and controls of the Sydney wave climate. *Int. J. Climatol.* **2010**, *30*, 1322–1335. [CrossRef]
58. Chowdhury, P.; Behera, M.R. Effect of long-term wave climate variability on longshore sediment transport along regional coastlines. *Prog. Oceanogr.* **2017**, *156*, 145–153. [CrossRef]
59. Kumar, V.S.; Naseef, T.M. Performance of ERA-interim wave data in the nearshore waters around India. *J. Atmos. Ocean Technol.* **2015**, *32*, 1257–1269. [CrossRef]